Robert J. M. van Geuns, MD
Piotr A. Wielopolski, PhD
Hein G. de Bruin, MD, PhD
Benno J. W. M. Rensing, MD, PhD
Marc Hulshoff, BSc
Peter M. A. van Ooijen, MSc
Pim J. de Feyter, MD, PhD
Matthijs Oudkerk, MD, PhD

Index terms:
Coronary angiography, 548.1244
Coronary vessels, MR, 548.121412, 548.121415, 548.121417, 548.12142
Coronary vessels, stenosis or obstruction, 548.76
Magnetic resonance (MR), vascular studies, 548.12142

Radiology 2000; 217:270–277

Abbreviations:
FLASH = fast low-angle shot
SNR = signal-to-noise ratio
3D = three-dimensional
VCATS = volume coronary angiography with targeted scans

[1] From the Departments of Cardiology, Thoraxcenter (R.J.M.v.G., B.J.W.M.R., M.H., P.J.d.F.) and Radiology, Daniel den Hoed Kliniek (P.A.W., H.G.d.B., P.M.A.v.O., M.O.), University Hospital Rotterdam, Groene Hilledijk 301, 3075 EA Rotterdam, the Netherlands. From the 1998 RSNA Scientific Assembly. Received July 28, 1999; revision requested September 1; revision received February 17, 2000; accepted April 4. **Address correspondence to** R.J.M.v.G. (e-mail: *vangeuns@card.azr.nl*).

Author contributions:
Guarantors of integrity of entire study, R.J.M.v.G., P.A.W., H.G.d.B., P.J.d.F., M.O.; study concepts and design, R.J.M.v.G., P.A.W., P.J.d.F., M.O.; definition of intellectual content, R.J.M.v.G., P.A.W., P.J.d.F., M.O.; literature research, R.J.M.v.G., P.A.W.; clinical studies, R.J.M.v.G., P.A.W., B.J.W.M.R.; experimental studies, P.A.W., R.J.M.v.G.; data acquisition, R.J.M.v.G., P.A.W., P.M.A.v.O.; data analysis, R.J.M.v.G., P.A.W., H.G.d.B., P.J.d.F., M.H., B.J.W.M.R.; statistical analysis, R.J.M.v.G., M.H.; manuscript preparation and editing, R.J.M.v.G., P.A.W.; manuscript review, R.J.M.v.G., P.A.W., H.G.d.B., P.J.d.F., M.O.

MR Coronary Angiography with Breath-hold Targeted Volumes: Preliminary Clinical Results[1]

PURPOSE: To assess the clinical value of a magnetic resonance (MR) coronary angiography strategy involving a small targeted volume to image one coronary segment in a single breath hold for the detection of greater than 50% stenosis.

MATERIALS AND METHODS: Thirty-eight patients referred for elective coronary angiography were included. The coronary arteries were localized during single-breath-hold, three-dimensional imaging of the entire heart. MR coronary angiography was then performed along the major coronary branches with a double-oblique, three-dimensional, gradient-echo sequence. Conventional coronary angiography was the reference-standard method.

RESULTS: Adequate visualization was achieved with MR coronary angiography in 85%–91% of the proximal coronary arterial branches and in 38%–76% of the middle and distal branches. Overall, 187 (69%) of 272 segments were suitable for comparison between conventional and MR coronary angiography. The diagnostic accuracy of MR coronary angiography for the detection of hemodynamically significant stenoses was 92%; sensitivity, 68%; and specificity, 97%. The sensitivity in individual segments was 50%–77%, whereas the specificity was 94%–100%.

CONCLUSION: Adequate visualization of the major coronary arterial branches was possible in the majority of patients. The observed accuracy of MR coronary angiography for detection of hemodynamically significant coronary arterial stenosis is promising, but it needs to be higher before this modality can be used reliably in a clinical setting.

Supplemental material: ***http://radiology.rsnajnls.org/cgi/content/full/217/1/270/DC1***

Magnetic resonance (MR) coronary angiography has undergone numerous developments during the past decade. Alternative techniques account for multiple two- and three-dimensional (3D) protocols with breath-hold and free-breathing approaches, or a combination of both (1–4). The clinical data reported (5–9) have been hampered mainly by technical problems that include blurring, long imaging times, inadequate coronary arterial coverage, and misregistration (10,11). We previously described a methodology to address some of these problems by using a breath-hold, targeted-volume imaging approach—that is, volume coronary angiography with targeted volumes (VCATS)—to image particular coronary arterial segments with reasonable resolution and thus identify hemodynamically significant stenoses (12). With targeted-volume imaging, data are acquired with optimal orientations along the coronary arterial branches of interest obtained from a single-breath-hold, low-resolution sequence for the entire volume of the heart. The purpose of this study was to assess the ability of VCATS to enable visualization of the major coronary arteries and the accuracy of this technique in the detection of stenosis, with conventional coronary angiography used as the standard of reference.

MATERIALS AND METHODS

Patients

The study population consisted of 38 patients (11 women, 27 men; age range, 43–72 years) who were referred for coronary angiography. Two cardiac research slots per week

TABLE 1
Routine Targeted Volumes Acquired and Coronary Segments

Volume No.	Coronary Segment Evaluated
1	Plane along LM, proximal LCX, and proximal LAD (transverse)
2	Plane of proximal RCA (transverse)
3	Plane along distal RCA and PDA (oblique)
4	Plane through aortic root and proximal RCA and LM (oblique)
5	Plane along LCX (oblique)
6	Plane along middle and distal LAD (oblique)
7	Plane along middle RCA (oblique)

Note.—LAD = left anterior descending coronary artery, LCX = left circumflex coronary artery, LM = left main coronary artery, PDA = posterior descending coronary artery, RCA = right coronary artery.

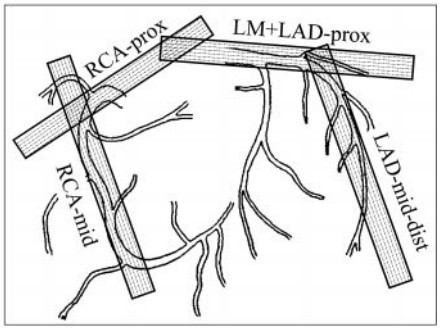

Figure 1. Drawing illustrates breath-hold 3D imaging of the coronary arteries with VCATS protocol. Different volumes are targeted for a detailed examination of selected coronary arterial segments. The major coronary segments can be imaged during seven breath holds. Four examples of possible angulations (rectangles) are illustrated. *dist* = distal, *LAD* = left anterior descending coronary artery, *LM* = left main coronary artery, *mid* = middle, *prox* = proximal, *RCA* = right coronary artery.

were available at our MR imaging site. Patients scheduled for elective coronary angiography were approached to participate in the MR coronary angiography study. The first two patients who agreed were scheduled to fill the available research slots. Exclusion criteria were previous coronary bypass surgery, intracoronary stent implantation, artificial pacemakers, intracranial clips, atrial fibrillation, severe claustrophobia, and severe lung disease that restricted breath-holding capability to less than 30 seconds. The study protocol was approved by our hospital committee on medical ethics and clinical investigation. Written informed consent was obtained from all patients prior to the MR imaging examinations.

MR Imaging

The studies were performed with a 1.5-T whole-body MR imaging system (Magnetom Vision; Siemens, Erlangen, Germany). Patients were placed in a supine position, and a four-channel quadrature phased-array body coil was placed over the thorax. Electrocardiographic electrodes were always set over the anterior part of the thorax and readjusted, if necessary, to obtain reasonable amplitude and clean signal trace in the monitoring unit after the patient was placed inside the magnet bore. After patient positioning, the magnetic field homogeneity over the thorax and heart was assessed to obtain uniform fat suppression in sequences that involved chemical shift fat suppression. This assessment was performed by comparing two three-plane, single-shot spin-echo train imaging (HASTE; Siemens) localizer sequences with and without a chemical shift fat suppression pulse applied. When the reduction of fat signal intensity was deemed inadequate, the shim currents were manipulated and the single-shot spin-echo train imaging localizer sequence with chemical shift fat suppression was repeated until satisfactory results were obtained.

To start the coronary localization procedure, a 3D single-breath-hold, multishot, segmented, echo-planar sequence was used to image the entire heart, with a 120-mm section obtained at end expiration. The data were subjected to multiplanar evaluation to determine the optimal imaging planes for the major coronary arterial branches (Table 1, Fig 1). This localization process has been described in detail previously (12). Seven orientations were obtained with multiplanar reformation before imaging with the breath-hold VCATS protocol proceeded.

Targeted-volume coronary angiography was performed with a 3D, double-oblique, segmented, gradient-echo—that is, turbo fast low-angle shot (TurboFLASH; Siemens)—sequence (5.3/2.3 [repetition time msec/echo time msec], incremental flip angle, 21 lines per segment, 110-msec acquisition window). A 24-mm-thick section (seven encoded partitions, 16 reconstructed by zero filling) was used with a 126×256 matrix and partial Fourier reconstruction. The imaging time was 21 heartbeats, and the imaging window coincided with middle-to-late diastole. The field of view was maintained constant at 240×320 mm^2, providing a resolution of $1.9 \times 1.25 \times 1.5$ mm^3. Magnetization transfer irradiation for myocardium-blood contrast-to-noise ratio enhancement (irradiation duration, 500 msec) and a single chemical shift fat suppression pulse were applied before data collection for each cardiac window. The orientation prescriptions were manually registered into the measurement platform for each targeted MR coronary angiogram. Breath holding was performed at end expiration to achieve position and plane reproducibility with respect to the multiplanar reformation data generated by using the volume localizer.

The breath-hold quality was assessed on every attempt by observing the ghost artifacts of the anterior thoracic wall over the heart. In case ghost artifacts appeared, repeated imaging of a particular volume was allowed. If severe ghost artifacts were present and the patient could not hold his or her breath adequately within four attempts, he or she was regarded as nonsuitable for the imaging procedure and thus excluded from the study.

To improve coronary arterial depiction on the volume localizer image, superparamagnetic iron oxide particles (AMI-25 [Endorem]; Laboratoire Guerbet, Roissy, France) were administered as a suspension containing 89.6 mg of iron (11.2 mg/mL) diluted in 100 mL of isotonic glucose solution. The solution was administered in a slow drop infusion for 30 minutes.

Conventional Coronary Angiography

All subjects underwent selective coronary arterial angiography by means of the Judkins technique (13) within 1 month before or after the MR examination. Two experienced cardiologists (B.J.W.M.R., P.J.d.F.) jointly interpreted the angiograms. The coronary tree was divided into proximal, middle, and distal segments according to American Heart Association guidelines (14). Under these guidelines, the left main coronary artery has a single segment. The proximal segment of the left anterior descending artery extends from the bifurcation to the first septal branch. The middle segment of the left anterior descending artery extends from the first to the third septal artery, whereas the distal segment extends from the third septal artery to the apex. The left circumflex coronary artery is divided into three segments by the first and second marginal branches. The proximal segment extends from the bifurca-

tion to the first marginal branch, the middle segment extends from the first to the second marginal branch, and the distal segment extends from the second marginal branch to the posterior lateral branch. The proximal right coronary artery extends from the origin to the first large acute marginal branch, the middle segment extends from the first to the third acute marginal branch, and the distal segment extends from the third acute marginal branch to the posterior descending branch. These segments were visually graded as either having no hemodynamically significant disease—that is, less than 50% diameter stenosis—or having hemodynamically significant disease—that is, greater than 50% diameter stenosis. In cases of disagreement, a third cardiologist made the final decision.

MR Image Interpretation

From each targeted volume, 16 source images in a dynamic loop (Movie 1, *http://radiology.rsnajnls.org/cgi/content/full/217/1/270/DC1*) were analyzed independently by a cardiologist (R.J.M.v.G.) and a radiologist (H.G.d.B.), who were unaware of the cardiac catheterization results. In cases of disagreement, consensus was achieved in a joint session with a third investigator (M.O.). Of all the coronary segments defined in the American Heart Association guidelines, only eight segments—those of the left main artery; proximal and middle left anterior descending arteries; proximal and middle left circumflex coronary arteries; and proximal, middle, and distal right coronary arteries—were included in this study. This selection resulted in the evaluation of 272 segments in 34 complete patient studies. These segments were regarded as assessable if overlapping structures (ie, veins, pericardium, and unsuppressed fat), image blurring, and/or ghost artifacts could be distinguished from the vessel itself. The segments included in more than one volume were finally evaluated in the volume with the best image quality. The assessable segments were graded as either not having hemodynamically significant diameter stenosis (<50%) or having hemodynamically significant stenosis (>50%).

To investigate the possibilities of integrating the coronary arterial path within a targeted volume into a single image, data sets were reconstructed by using a volume-rendering program (VOXELVIEW; Vital Images, Minneapolis, Minn) that was run on a dedicated graphic workstation (Indigo2; Silicon Graphics, Mountain View, Calif). Segmentation was required to eliminate unwanted structures and view the coronary segment from any viewing angle and thus better assess the presence of any detected stenoses at the initial review. Volume-rendered data were not evaluated for their additional diagnostic value, but rather this technique was used strictly as an exploratory tool to conjecture about the possible likeness of volume-rendered images to the corresponding coronary angiograms.

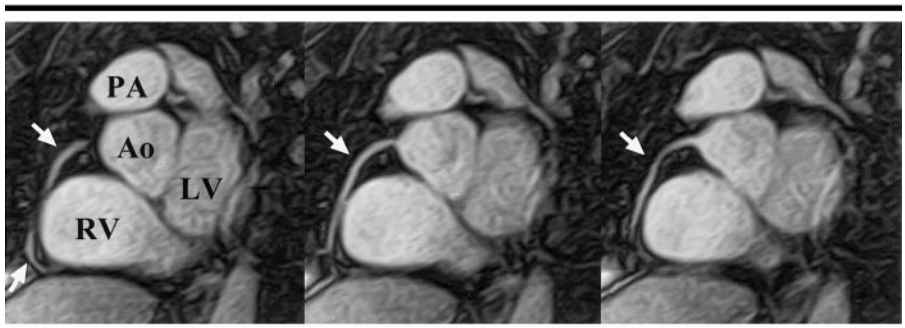

a.

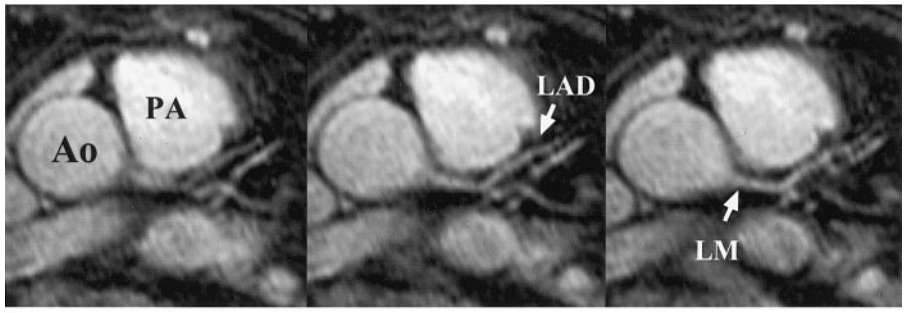

b.

Figure 2. In **a** and **b**, *Ao* = aorta, *PA* = pulmonary artery. **(a)** Double-oblique, 3D, breath-hold, segmented, gradient-echo MR images (TurboFLASH, 5.3/2.3, incremental flip angle, 21 lines per segment, 110-msec acquisition window, 1.9 × 1.25 × 1.5-mm resolution with interpolation by zero filling) of the middle segment of the right coronary artery in a 43-year-old man. Three consecutive sections show the continuation of a nondiseased tortuous vessel (arrows) through the volume. *LV* = left ventricle, *RV* = right ventricle. **(b)** Transverse targeted-volume images of the left main (*LM*) and proximal left anterior descending (*LAD*) arteries in a 45-year-old woman.

TABLE 2
Assessability of Different Coronary Arterial Segments with MR Coronary Angiography

Segment	Assessability*
Proximal RCA	29 (85)
Middle RCA	22 (65)
Distal RCA	17 (50)
LM	31 (91)
Proximal LAD	31 (91)
Middle LAD	26 (76)
Proximal LCX	18 (53)
Middle LCX	13 (38)

* Data are numbers of patients in whom the given segment was assessable with MR coronary angiography, based on a total of 34 patients. Numbers in parentheses are percentages. LAD = left anterior descending coronary artery, LCX = left circumflex coronary artery, LM = left main coronary artery, RCA = right coronary artery.

TABLE 3
Relation between Angiographic Status of Coronary Arterial Segments and Assessability at MR Coronary Angiography

MR Imaging	Lesion Absent at Angiography	Lesion Present at Angiography	Total
Assessable	156	31	187
Nonassessable	75	10	85
Total	231	41	272

Note.—Data are numbers of coronary arterial segments.

Statistical Analyses

Conventional coronary angiography served as the standard of reference for determining the diagnostic value of MR coronary angiography. The diagnostic value for the detection of hemodynamically significant (>50% diameter) stenosis in a segment was expressed in sensitivity, specificity, positive predictive, negative predictive, and diagnostic accuracy values.

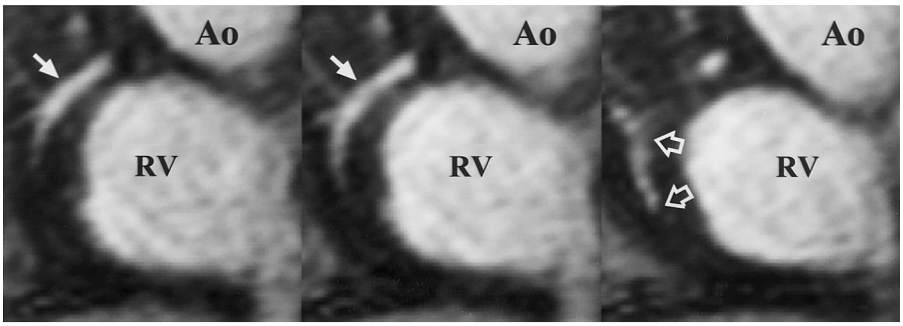

a.

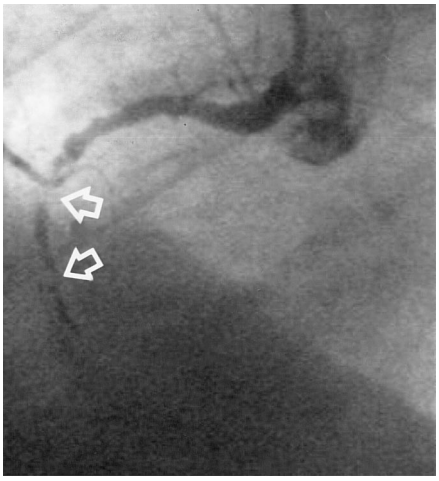

b.

Figure 3. **(a)** Double-oblique 3D breath-hold segmented gradient-echo images (Turbo-FLASH, 5.3/2.3, incremental flip angle, 21 lines per segment, 110-msec acquisition window, 1.9 × 1.25 × 1.5-mm resolution with interpolation by zero filling) of the right coronary artery (solid arrows) in a 72-year-old man. Three consecutive sections demonstrate the presence of hemodynamically significant stenoses (open arrows) followed by complete occlusion. *Ao* = aorta, *RV* = right ventricle. **(b)** Corresponding conventional coronary angiogram shows the stenoses (arrows).

RESULTS

The mean interval (± SD) between cine-mode angiography and MR coronary angiography was 10 days ± 7. In four of the 38 patients who agreed to participate in this study, the MR examination was not completed owing to hardware problems ($n = 1$), unexpected claustrophobia ($n = 2$), or inability to suspend respiration for 21 heartbeats according to the study design ($n = 1$). Thus, MR imaging studies were performed in the remaining 34 subjects with minor technical, operational, and patient-related problems. The mean attempted number of volumes (± SD) collected per patient was 10.0 ± 2.3.

The minor technical difficulties included problems performing good electrocardiographic tracing in three (9%) patients and mistriggering from imaging gradient–induced interference in some volume orientations in 30 (8.8%) of 340 measurements. Incomplete fat suppression within the set of volumes collected per patient was always present to a certain degree, and it was prevalent in the distal portion of the left anterior descending artery. Operational problems included input errors in the volume orientation prescription in eight (2.4%) of 340 measurements. Patient-related problems were those due to an inconsistent breath-hold position with respect to the volume localizer in 17 (5.0%) of 340 measurements and incomplete acquisition of all targeted volumes in two patients (five [1.5%] of 340 measurements).

Because of the fast feedback on the data acquired, corrections were directly applied to acquire the desired volume; this resulted in 100% data collection in the segments studied. The mean (± SD) breath-hold time per acquired targeted volume was 23 seconds ± 4. The acquisition of the volume localizer image, selection of the optimal plane location and orientation of the targeted volumes with multiplanar reformation, and acquisition of the targeted-volume images were consistently completed in less than 30 minutes. Of the 272 possible coronary arterial segments in the 34 patients, 187 (69%) were deemed to be assessable by using MR coronary angiography. The range of assessability varied substantially, from 91% for the left main coronary artery to 38% for the middle left circumflex coronary artery. The resultant data on the assessability of individual segments are listed in Table 2.

The conventional coronary angiograms showed hemodynamically significant stenosis in 23 patients—three-vessel disease in three patients, two-vessel disease in 10, and single-vessel disease in another 10. Overall, 41 stenoses were present in the eight major coronary arterial branches. Thirty-one of these stenoses were located in the 187 assessable segments, and 10 were in the nonassessable segments (Table 3). Two examples of targeted-volume images of nondiseased vessels are shown in Figure 2. Examples of two stenoses in the right coronary artery are shown in Figure 3. An example of stenosis of the left anterior descending artery segment is shown in Figure 4.

The findings for the detection of hemodynamically significant stenosis (>50% of observable diameter) are summarized in Table 4. The sensitivity of MR coronary angiography ranged from 50% to 77%, and the specificity ranged from 94% to 100%. The overall sensitivity and specificity were 68% and 97%, respectively, with an accuracy of 92%.

DISCUSSION

Despite all the technical improvements in MR imaging during the past decade, MR coronary angiography remains a challenging clinical investigation. Many techniques have been explored to date; these include two-dimensional breath-hold, single-section, gradient-echo and 3D free-breathing, respiratory-gated, gradient-echo acquisitions. These techniques have their advantages and disadvantages. Although two-dimensional breath-hold techniques are fast and provide immediate feedback to the imaging operator, image and section misregistration between several acquired sections along a coronary arterial segment of interest can lead to an inaccurate measurement of stenosis in a tortuous coronary segment. This problem has been addressed by using free-breathing MR coronary angiography (ie, retrospective and prospective gated navigator 3D imaging) techniques that enable imaging of a larger volume with a better signal-to-noise ratio (SNR) and good data consistency for diagnosis in a 3D reconstruction platform after data have been acquired (using multiplanar reformation or volume rendering). Nonetheless, free-breathing MR coronary angiography has a major drawback in terms of acquisition slowness, which results in poor operator feedback in cases in which imaging must be repeated when image detail loss occurs owing to an inconsistent respiratory pattern during the acquisition. However, MR imaging operator expertise is less relevant with 3D mea-

surements than with two-dimensional breath-hold measurements.

In this work, we evaluated our initial clinical experience with a breath-hold VCATS protocol that aims to address some of the known difficulties with MR coronary angiography described earlier. Breath-hold acquisitions reduce breathing artifacts, whereas the use of a small imaging volume yields the data consistency required to evaluate MR coronary angiographic data sets for specific coronary segments. In addition, with the 3D nature of the VCATS measurement sequence described, there is the potential to compensate for the SNR loss in faster acquisition scenarios. Nonetheless, all MR coronary angiography techniques must account for the superposition of motion of the coronary vessels during cardiac contraction, which leads to the loss of image detail, and the resolution and SNR deficiencies that are inherent to MR imaging and limit the accurate depiction of the small caliber of the coronary vessels and possible stenoses. Because images are formed from composite data collected during many heartbeats, slow or sudden alterations in the cardiac rhythm during the acquisitions can lead to additional loss of vessel detail.

Breath-hold MR coronary angiography was possible in the majority of patients in this study. Patients with known severe pulmonary disease were excluded in the selection process; this resulted in the acquisition of more reproducible data from cooperative individuals. The free-breathing MR coronary angiography technique with navigator gating may have been a suitable imaging alternative in the excluded patient population. Claustrophobia and inadequate electrocardiographic tracing—the latter of which is associated with small amplitude of the R wave and prone to interference from imaging gradient activity—were among the factors that resulted in the late exclusion of patients and reduced efficiency during imaging. These limitations may improve with the availability of short-bore dedicated cardiac MR imaging systems and optical-transmission electrocardiographic electrodes (15,16).

We believe that in this study with the described MR coronary angiography technique, we achieved a promising level of sensitivity and specificity in the detection of hemodynamically significant coronary arterial stenosis in the symptomatic patient group that was selected. Such patients have a high preexamination likelihood of having coronary arterial stenosis. In general, it is impossible to predict the sensitivity and specificity of a diagnostic examination in patients who are less strictly selected. In addition, the results could have changed substantially with the exclusion of nonassessable segments. This was hinted at by the number of stenoses detected by using VCATS—only 21 (51%) of the 41 stenoses detected in total at conventional angiography.

Additional points regarding the study setup must be clarified. The MR sequence selected for VCATS is not without limitations. First, the SNR that is considered adequate for diagnosis limits the submillimeter resolution that is possible with the described sequence (minimum true voxel size for 21 heartbeats, 1.30 × 0.95 × 2.5 mm^3). In practice, an image with lower resolution is feasible, and only vessels with a diameter larger than approximately 2 mm are suitable for evaluation. At present, with conventional coronary angiography, a resolution of 0.1 mm can be obtained and stenoses of high (>70%) and moderate (50%–70%) grades can be differentiated. Therefore, with the current resolution

TABLE 4
Diagnostic Accuracy of MR Coronary Angiography for Detection of Greater than 50% Diameter Stenosis

Segment	No. of Segments Visualized*	No. of Stenoses	Sensitivity (%)	Specificity (%)	PPV (%)	NPV (%)	Accuracy (%)
LM + LAD	88 (86)	13	77	97	83	96	94
RCA	68 (67)	14	64	94	75	91	88
LCX	31 (46)	4	50	100	100	93	94
Overall	187 (69)	31	68	97	81	94	92

Note.—LAD = left anterior descending coronary artery, LCX = left circumflex coronary artery, LM = left main coronary artery, NPV = negative predictive value, PPV = positive predictive value, RCA = right coronary artery.

* Data are the combined numbers of segments that could be assessed at MR coronary angiography (see Table 2). Numbers in parentheses are percentages, calculated by averaging the sum of percentages for a given segment in Table 2.

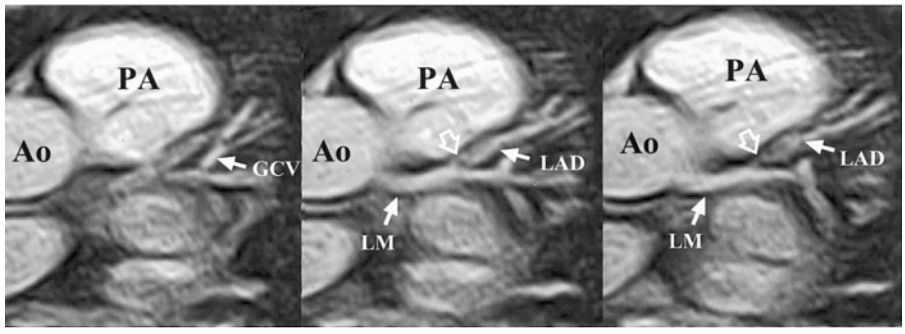

a.

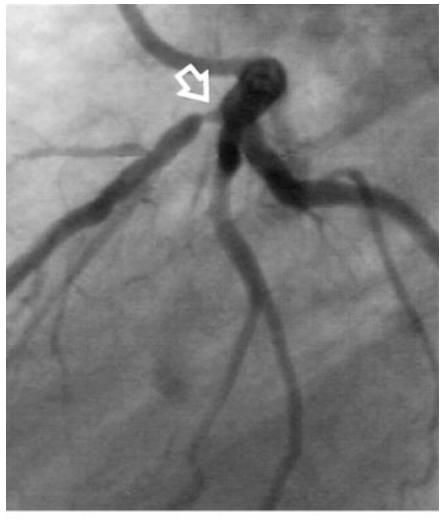

b.

Figure 4. **(a)** Transverse, 3D, segmented, gradient-echo images (TurboFLASH, 5.3/2.3, incremental flip angle, 21 lines per segment, 110-msec acquisition window, 1.9 × 1.25 × 1.5-mm resolution with interpolation by zero filling) of stenosis (open arrows) of a proximal left anterior descending coronary artery (*LAD*) in a 51-year-old man. *Ao* = aorta, *GCV* = great cardiac vein, *LM* = left main coronary artery, *PA* = pulmonary artery. **(b)** Corresponding conventional coronary angiogram shows the stenosis (arrow).

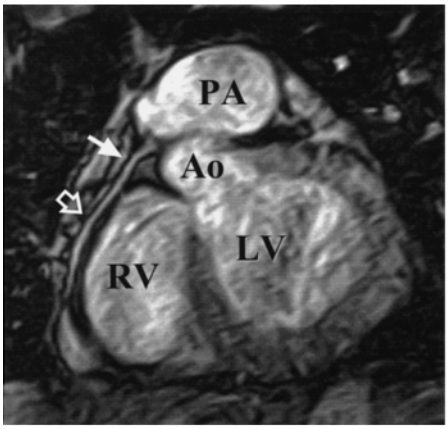

a.

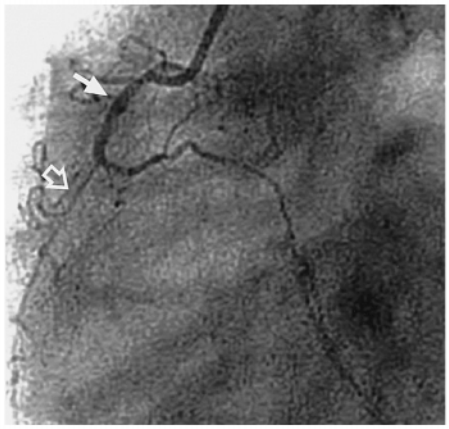

b.

Figure 5. False-negative findings of stenosis. **(a)** Double-oblique, 3D, breath-hold, segmented, gradient-echo image (TurboFLASH, 5.3/2.3, incremental flip angle, 21 lines per segment, 110-msec acquisition window, 1.9 × 1.25 × 1.5-mm resolution with interpolation by zero filling) of the right coronary artery in a 44-year-old woman. The clearly delineated vessel (arrows) seems to be patent for at least 5 cm. *Ao* = aorta, *LV* = left ventricle, *PA* = pulmonary artery, *RV* = right ventricle. **(b)** Corresponding conventional coronary angiogram shows the vessel in **a** (open and solid arrows) with an occluded middle segment (open arrow).

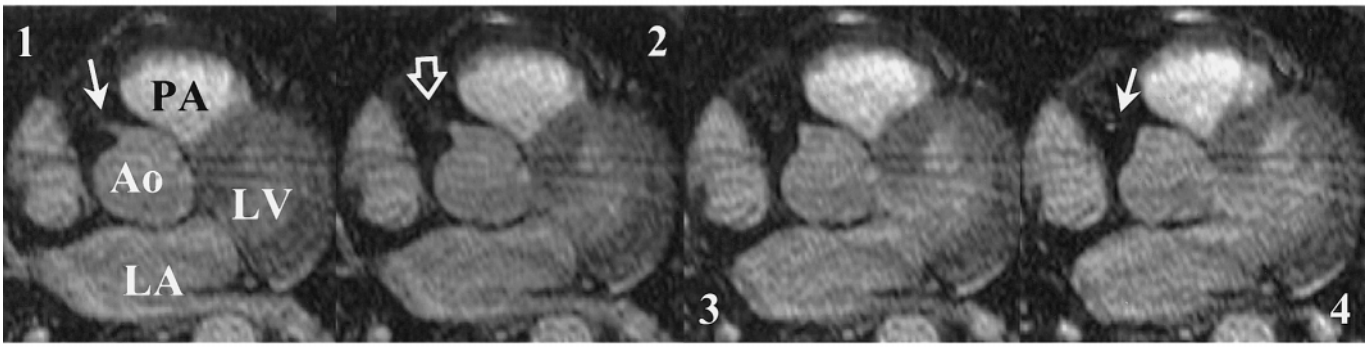

a.

b.

Figure 6. False-positive findings of stenosis. **(a)** Transverse, 3D, segmented, gradient-echo images (TurboFLASH, 5.3/2.3, incremental flip angle, 21 lines per segment, 110-msec acquisition window, 1.9 × 1.25 × 1.5-mm resolution with interpolation by zero filling) through the proximal right coronary artery in a 71-year-old man. On four consecutive sections, the right coronary artery seems to be occluded (open arrow) beyond 0.5 cm of its origin (solid arrows) owing to incomplete fat suppression and partial Fourier reconstruction. *Ao* = aorta, *LA* = left atrium, *LV* = left ventricle, *PA* = pulmonary artery. **(b)** Corresponding conventional coronary angiogram shows the vessel to be patent.

setting in the VCATS protocol, no specific grading of MR angiograms can be attempted.

Second, our MR coronary angiography technique and that of many others are proton density weighted in nature (due to the long magnetization recovery period between data acquisitions, the presence of inflow, and imaging with an incremented flip angle series), despite the additional application of magnetization transfer contrast irradiation to improve myocardial and perhaps plaque signal suppression. Therefore, false-negative results (Figure 5) can be expected, with a normal appearance of the coronary segment at MR coronary angiography and complete occlusion on the corresponding conventional coronary angiogram. The effects of magnetization transfer contrast irradiation on atherosclerotic plaque have been investigated by Pachot-Clouard et al (17). This group suggests that magnetization transfer contrast irradiation–induced signal drop occurs in atherosclerotic plaque components with an effect that is more pronounced for the fibrous cap and media than for the lipid core and adventitia. Nonetheless, with the present setup, in which triggered images are used, it is difficult to define the exact contribution of magnetization transfer contrast irradiation in signal attenuation from plaque for different cardiac rates.

Third, it was difficult to achieve complete fat suppression in all coronary segments. Remnant nonsuppressed fat can induce particular artifacts, such as blurring, vessel shift, and thin dark lines when partial Fourier reconstruction is used. These artifacts can have a major role in the diagnosis of particular coronary segments and, if the reader is not well aware of the limitations, render a segment nonassessable, as demonstrated in a false-positive case in our study (Fig 6).

The addition of the partially intravascular superparamagnetic iron oxide contrast medium produced some T1 shortening in blood; however, this may not substantially change the resultant SNR

using a small targeted volume mainly obtained with proton density weighting, in which enough longitudinal magnetization recovery and inflow effects combined reduce the overall effectiveness of any contrast medium that is present in blood. The T1 shortening obtained did provide substantially better SNR results on the volume localizer images, because a larger volume of blood was saturated with every heart cycle and inflow effects of fully magnetized blood spins were not expected. The superparamagnetic iron oxide contrast medium remains approximately 10%–20% intravascular, with an approximate T1 relaxation time of 400–700 msec, which is stable for several hours after the initial infusion.

Visualization of the left circumflex coronary artery is difficult with all MR coronary angiography techniques, and the present protocol cannot completely solve this problem. One problem arises from the lower SNR caused by the relatively large distance between the left circumflex coronary artery and the surface coils placed around the chest wall. In addition, the close relation between the left circumflex coronary artery, the coronary sinus, and the auricle of the left atrium hampers evaluation of the vessel owing to the lack of resolution and insufficient SNR and contrast-to-noise ratio. Furthermore, the application of magnetization transfer contrast irradiation for an improved contrast-to-noise ratio between the myocardium and blood pools is not without consequences. Magnetization transfer contrast irradiation increases the specific absorption ratio in the patient and reduces the SNR that may be achievable in blood without its application.

The application of volume rendering techniques makes it possible to integrate the 3D course of a coronary segment on a single image. This appears to be useful for delineating the coronary anatomy, as demonstrated in Figures 7–9 (Movies 2,3; *http://radiology.rsnajnls.org/cgi/content/full/217/1/270/DC1*), and helping to identify coronary lesions from any viewing angle. Nonetheless, postprocessing adds appreciable time to the overall examination. Data transfer to a specialized workstation and the preparation of data by segmenting the unwanted structures before acquiring the final volume-rendered image can be time consuming. Manual segmentation requires 5–15 minutes for each volume; therefore, no attempt was made to render all seven volumes collected in each patient. However, the use of improved software may substantially reduce this manipulation time to make this display utility suitable for routine use.

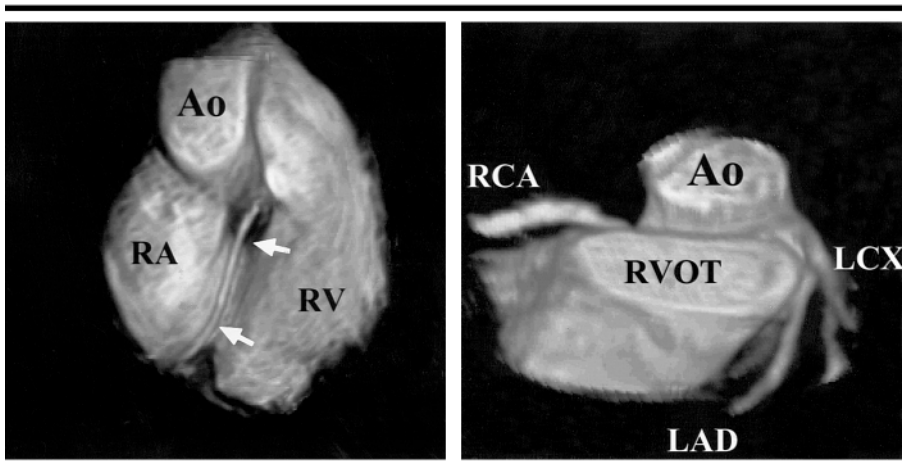

a. **b.**

Figure 7. **(a)** Right anterior, volume-rendered, double-oblique, 3D, breath-hold, segmented, gradient-echo image (TurboFLASH, 5.3/2.3, incremental flip angle, 21 lines per segment, 110-msec acquisition window, 1.9 × 1.25 × 1.5-mm resolution with interpolation by zero filling) of a targeted volume of a nondiseased right coronary artery (arrows) in a 43-year-old man. *Ao* = aorta, *RA* = right atrium, *RV* = right ventricle. **(b)** Anterior cranial volume-rendered image of a targeted volume of the aortic root in the same patient. *Ao* = aorta, *LAD* = left anterior descending coronary artery, *LCX* = left circumflex coronary artery, *RCA* = right coronary artery, *RVOT* = right ventricular outflow tract.

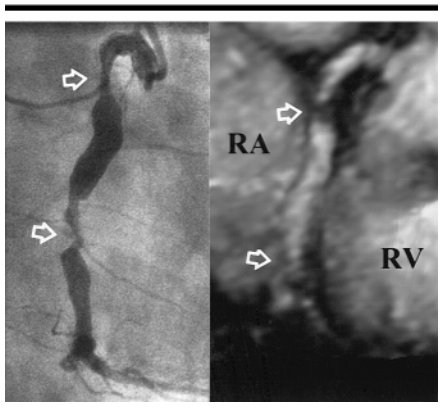

Figure 8. Right anterior, volume-rendered, double-oblique, 3D, breath-hold, segmented, gradient-echo image (TurboFLASH, 5.3/2.3, incremental flip angle, 21 lines per segment, 110-msec acquisition window, 1.9 × 1.25 × 1.5-mm resolution with interpolation by zero filling) (right) and corresponding conventional coronary angiogram (left) of a targeted volume of a right coronary artery in a 57-year-old man show two hemodynamically significant stenoses (arrows). *RA* = right atrium, *RV* = right ventricle.

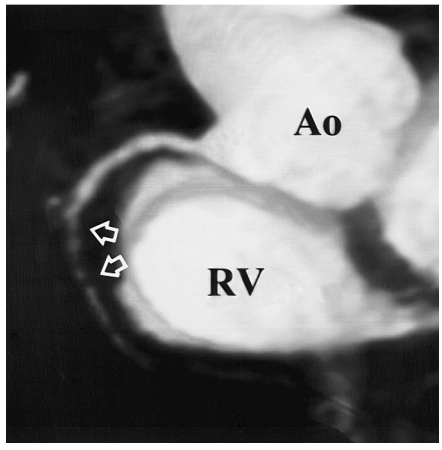

Figure 9. Anterior volume-rendered image (1.9 × 1.25 × 1.5-mm resolution with interpolation by zero filling) of the right coronary artery in the patient in Figure 3 with hemodynamically significant stenoses (arrows) followed by complete occlusion. *Ao* = aorta, *RV* = right ventricle.

In total, 72 targeted volumes in 25 patients were reconstructed with volume rendering and believed to enable proper visualization of the coronary segment in question compared with conventional angiography. The settings for the voxel opacity (or transparency) were manipulated to demonstrate an appearance of features similar to that on conventional angiograms, because the effects of the signal intensity distribution observed during review of individual sections of the corresponding VCATS volume were not known a priori. Therefore, the volume-rendered data on the diseased vessels presented in Figures 8 and 9 were obtained retrospectively on the basis of findings on the conventional angiograms. This procedure was feasible in this preliminary study because the volume rendering technique is fairly new and has not been adequately assessed for MR im-

aging data sets, especially with signal intensity histograms and signal intensity ranges that are different in each targeted coronary volume. This is in contrast to the more routine volume rendering processing performed on CT data, in which attenuation value ranges (in HU) in tissues are predictable to well known and, in turn, provide a well-defined intensity histogram. However, MR data are heavily dependent on the reception pattern of the coil array surrounding the thorax—that is, dependent on patient size. No attempts to correct the signal intensity profile of each phased-array coil and thus homogenize the image data were made; therefore, the volume rendering settings were an operator-related choice.

In spite of many measurement difficulties, the visualization on and quality of the images in this initial evaluation were encouraging enough to warrant continued, more extensive clinical trials with the proposed VCATS methodology. The proposed protocol is practical for a clinical setup and provides the means for fast assessment of the coronary arteries with acquisition times of less than 30 minutes. We envision that further improvements in the presently used MR pulse sequence that yield better signal-to-noise and contrast-to-noise ratios and better resolution with a shorter breath-hold time will substantially help increase the sensitivity and specificity of the approach. On the basis of theoretical estimates (18), the addition of intravascular contrast media that provide very short T1 relaxation times in blood (<40 msec) can facilitate some of the improvements (19) needed to consider the routine use of a VCATS protocol for the evaluation of coronary arteries. Furthermore, contrast media may improve the differentiation between the vessel lumen and coronary arterial wall by enabling the acquisition of only a luminogram.

In conclusion, the described VCATS protocol makes it possible to localize the major coronary arterial branches in a short examination time, and the observed degree of accuracy in the detection of hemodynamically significant stenoses within these branches is encouraging. The selected measurement sequence for VCATS needs improved SNR and spatial resolution with shorter measurement times to facilitate a more adequate scenario for coronary arterial assessment on a broader scale. We envision that further refinements in the hardware and software in MR cardiac machines and the introduction of T1-efficient intravascular contrast media will considerably augment the dependability of the proposed methodology.

References

1. Edelman RR, Manning WJ, Burstein D, Paulin S. Coronary arteries: breath-hold MR angiography. Radiology 1991; 181: 641–643.
2. Wang Y, Grimm RC, Rossman PJ, Debbins JP, Riederer SJ, Ehman RL. 3D coronary MR angiography in multiple breath-holds using a respiratory feedback monitor. Magn Reson Med 1995; 34:11–16.
3. Li D, Kaushikkar S, Haacke EM, et al. Coronary arteries: three-dimensional MR imaging with retrospective respiratory gating. Radiology 1996; 201:857–863.
4. McConnell MV, Khasgiwala VC, Savord BJ, et al. Prospective adaptive navigator correction for breath-hold MR coronary angiography. Magn Reson Med 1997; 37: 148–152.
5. Manning WJ, Li W, Edelman RR. A preliminary report comparing magnetic resonance coronary angiography with conventional angiography. N Engl J Med 1993; 328:828–832.
6. Duerinckx AJ, Urman MK. Two-dimensional coronary MR angiography: analysis of initial clinical results. Radiology 1994; 193:731–738.
7. Pennell DJ, Bogren HG, Keegan J, Firmin DN, Underwood SR. Assessment of coronary artery stenosis by magnetic resonance imaging. Heart 1996; 75:127–133.
8. Post JC, van Rossum AC, Hofman MB, de Cock CC, Valk J, Visser CA. Clinical utility of two-dimensional magnetic resonance angiography in detecting coronary artery disease. Eur Heart J 1997; 18:426–433.
9. van Geuns RJM, de Bruin HG, Wielopolski PA, et al. MRI of the coronary arteries: clinical evaluation from three-dimensional evaluation of a respiratory gated technique. Heart 1999; 82:515–519.
10. Post JC, van Rossum AC, Hofman MB, Valk J, Visser CA. Three-dimensional respiratory-gated MR angiography of coronary arteries: comparison with conventional coronary angiography. AJR Am J Roentgenol 1996; 166:1399–1404.
11. Duerinckx AJ, Atkinson DP, Mintorovitch J, Simonetti OP, Vrman MK. Two-dimensional coronary MRA: limitations and artifacts. Eur Radiol 1996; 6:312–325.
12. Wielopolski P, van Geuns R, de Feyter P, Oudkerk M. Breath-hold coronary MR angiography with volume targeted imaging. Radiology 1998; 209:209–219.
13. Judkins MP. Selective coronary arteriography. I. A percutaneous transfemoral technique. Radiology 1967; 89:815–824.
14. Austen WG, Edwards JE, Frye RL, et al. A reporting system on patients evaluated for coronary artery disease: report of the Ad Hoc Committee for Grading of Coronary Artery Disease, Council on Cardiovascular Surgery, American Heart Association. Circulation 1975; 51(suppl):5–40.
15. Felblinger J, Lehmann C, Boesch C. Electrocardiogram acquisition during MR examinations for patient monitoring and sequence triggering. Magn Reson Med 1994; 32:523–529.
16. Felblinger J, Debatin JF, Boesch C, Gruetter R, McKinnon GC. Synchronization device for electrocardiography gated echo-planar imaging. Radiology 1995; 197:311–313.
17. Pachot-Clouard M, Vaufrey F, Darrasse L, Toussainti JF. Magnetization transfer characteristics in atherosclerotic plaque components assessed by adapted binomial preparation pulses. MAGMA 1998; 7:9–15.
18. Johansson LO, Fischer SE, Lorenz CH. Benefit of T1 reduction for magnetic resonance coronary angiography: a numerical simulation and phantom study. J Magn Reson Imaging 1999; 9:552–556.
19. Lauffer RB, Parmelee DJ, Dunham SU, et al. MS-325: albumin-targeted contrast agent for MR angiography. Radiology 1998; 207:529–538.